Materials Research Innovations

ISSN: 1432-8917 (Print) 1433-075X (Online) Journal homepage: https://www.tandfonline.com/loi/ymri20

Combustion synthesis of Fe_3O_4/mesorporous carbon composite for lithium ion battery anode

Qingtang Zhang, Yan Meng & Xiaomei Wang

To cite this article: Qingtang Zhang, Yan Meng & Xiaomei Wang (2019) Combustion synthesis of Fe_3O_4/mesorporous carbon composite for lithium ion battery anode, Materials Research Innovations, 23:7, 407-412, DOI: 10.1080/14328917.2018.1505681

To link to this article: https://doi.org/10.1080/14328917.2018.1505681

MATERIALS RESEARCH INNOVATIONS
2019, VOL. 23, NO. 7, 407–412
https://doi.org/10.1080/14328917.2018.1505681

Taylor & Francis
Taylor & Francis Group

Combustion synthesis of Fe_3O_4/mesorporous carbon composite for lithium ion battery anode

Qingtang Zhang, Yan Meng and Xiaomei Wang

State Key Laboratory of Advanced Processing and Recycling of Non-ferrous Metals, School of Petrochemical Engineering, Lanzhou University of Technology, Lanzhou, China

ABSTRACT

Fe_3O_4/mesorporous carbon (Fe_3O_4-MC) composite is prepared by a combustion synthesis from the mixture of MC, $Fe(NO_3)_3 \cdot 9H_2O$ and $Fe(CH_3COO)_2 \cdot 4H_2O$ under the argon follow. XRD result proves that Fe_3O_4 crystals are being in the Fe_3O_4-MC composite. The SEM indicate MC are covered by Fe_3O_4 nanoparticles. TEM reveal that Fe_3O_4 nanoparticles can be obtained by using pyrolysis of ferric salt adsorbed MC. BET analysis proves that the specific surface area of Fe_3O_4-MC composite is distinctly lower than that of MC, indicating some pores of MC are filled by Fe_3O_4 nanoparticles. The above novel structure is beneficial to improving the electrochemical performance. Fe_3O_4-MC composite exhibits a high reversible capacity (920 mAh· g^{-1} at 100 mA· g^{-1}), good rate behavior (281 mAh· g^{-1} at 1500 mA· g^{-1}).

ARTICLE HISTORY
Received 17 April 2018
Accepted 25 July 2018

KEYWORDS
Mesoporous carbon; combustion synthesis; Fe_3O_4; nanoparticles; lithium ion battery

1. Introduction

Lithium-ion batteries (LIBs), with high energy and power densities, long cycle life and relatively low self-discharge, have been considered as one of the most prospective power sources for portable electronics and electric vehicles over the past two decades [1–4]. The theoretical capacity of traditional graphite carbon is only 372 mAh· g^{-1} [5–7]. So, graphite carbon cannot meet the increasing demands of high capacity anode materials for advanced LIBs. Therefore, tremendous efforts have been devoted to seeking for novel anode materials with high capacity to construct advanced LIBs.

Transition metal oxides (TMOs) with higher theoretical capacity are considered as the promising anode materials for LIBs [8–11]. Among them, Fe_3O_4 has received considerable attention, owing to its various advantages, including high theoretical capacity (927 mAh· g^{-1}), earth abundance, low cost and eco-friendly [12,13]. Nevertheless, due to the intrinsic poor electronic conductivity, huge volume changes and pulverization during repeated lithium insertion/extraction, Fe_3O_4 anode materials usually face fast capacity fading [14,15]. To resolve these problems, many strategies have been intensively developed to enhance the electrochemical performance by designing different Fe_3O_4 structures, including Fe_3O_4/C nanosheets [16], hollow Fe_3O_4/C microspheres [17], carbon-encapsulated Fe_3O_4 nanoparticles [18], Fe_3O_4/C composites [19–23], carbon-decorated single-crystalline Fe_3O_4 nanowires [24] and Fe_3O_4/carbon core-shell nanotubes [25]. Apparently, the compositing of Fe_3O_4 with conductive carbon has been regarded as a viable and effective ways to ameliorate the conductivity of composite materials. In addition, carbon with specific characteristics, such as the mesoporous properties, can absorb the volume changes through the adsorption process making Fe_3O_4 into the hole of carbon, further improving the rate and cycling performance of Fe_3O_4 as the anode materials for lithium ion batteries.

In recent years, mesoporous carbon (MC) has been playing a crucial role as an excellent electrode material for capacitor because of its overwhelming advantages, for example, controllable meso/microporosity, large specific surface area and good electronic conductivity [26–28]. In fact, commercial MC has been widely used to make composite electrode materials for LIBs, which can effectively provide buffer lithium ions for rapid electrochemical reactions. In addition, combustion synthesis is feasible way to get metal nanoparticles [29,30]. Herein, we combine MC and combustion synthesis together to prepare Fe_3O_4-MC composite. The mixture of MC, $Fe(NO_3)_3 \cdot 9H_2O$ and $Fe(CH_3COO)_2 \cdot 4H_2O$ were heated and self-sustained reactions occur to form Fe_3O_4-MC composite. The Fe_3O_4-MC composite exhibits a high reversible capacity (920 mAh· g^{-1} at 100 mA· g^{-1}) and excellent rate performance (281 mAh· g^{-1} at 1500 mA· g^{-1}), which is far superior to those of bare Fe_3O_4.

2. Experimental

2.1 *Sample preparation*

MC (Ningde Xinsen, Fujian), $Fe(NO_3)_3 \cdot 9H_2O$ and $Fe(CH_3COO)_2 \cdot 4H_2O$ were used without further purification. To synthesize Fe_3O_4-MC composite, 3.0054 g $Fe(NO_3)_3 \cdot 9H_2O$ and 0.7080 g $Fe(CH_3COO)_2 \cdot 4H_2O$ were dissolved in ethanol with assistance of vigorously stirring (the molar ratio of $Fe(NO_3)_3 \cdot 9H_2O$ to $Fe(CH_3COO)_2 \cdot 4H_2O$ was fixed as 2:1) and the as-obtained solution was adsorbed by 0.15 g MC, and followed by drying. Then, the dried precursor was heated at 550°C for 4 h in flowing Ar to obtain Fe_3O_4-MC composite. To prepare bare Fe_3O_4 as comparison, the synthesis was carried out without MC under the same conditions like Fe_3O_4-MC composite.

CONTACT Xiaomei Wang wxmei06@163.com State Key Laboratory of Advanced Processing and Recycling of Non-ferrous Metals, School of Petrochemical Engineering, Lanzhou University of Technology, Lanzhou, 730050 China

2.2 *Characterization*

CR2032 coin cells were assembled determine the electrochemical properties of bare Fe_3O_4 and Fe_3O_4-MC composite as anode materials in lithium ion cells. The working electrode were fabricated by mixing 80% active materials (bare Fe_3O_4, Fe_3O_4-MC composite), 10% super p, and 10% aqueous LA132 binder (Chengdu Indigo power sources CO., Ltd.). All the cells were assembled with the bare Fe_3O_4 or Fe_3O_4-MC composite as test electrode, lithium flake as counter electrode and the polypropylene film (celgard 2400) as separator in a high-purity argon-filled glovebox. The electrolyte was 1 mol/L $LiPF_6$ in dimethyl carbonate/ethyl-methyl carbonate/ethylene carbonate (1:1:1). Charge-discharge tests were carried out galvanostatically over a voltage range of 0.0–3.0 V in a CT2001A LAND battery test system (Wuhan, China). Cyclic voltammentry curves were recorded on a ZF100 electrochemical workstation (Shanghai Zhengfang Electronics Co., Ltd). Electrochemical impedance spectroscopic (EIS) measurements were performed with a CHI660D electrochemical workstation (Shanghai Chenhua Instruments Co., China). All measurements were carried out at room temperature.

The morphologies of MC and Fe_3O_4-MC composite were characterized by scanning electron microscopy (SEM) (JSM-6700F, Japan). The energy dispersive spectroscopy (EDS) was performed to determine the elemental composition analysis of Fe_3O_4-MC composite. The morphology of bare Fe_3O_4 and Fe_3O_4-MC composite was further examined by high resolution transmission electron microscopy (TEM) (JEOL JSM 2100F). The crystalline structure of bare Fe_3O_4, MC and Fe_3O_4-MC composite were studied by X-ray diffraction (XRD) (RINT2000, Cu kα, λ = 0.154 nm). The porous properties of Fe_3O_4-MC composite were estimated by nitrogen adsorption/desorption analyses at 77 K.

3. Results and discussion

The XRD patterns of bare Fe_3O_4, MC and Fe_3O_4-MC composite are shown in Figure 1. The characteristic peaks of bare Fe_3O_4 and Fe_3O_4-MC composite appear at 2θ = 18.2°, 30.0°, 35.4°, 43.0°, 53.4°, 56.9°, 62.5°and 73.9°, which are perfectly indexed to the (111), (220), (311), (400), (422), (511), (440) and (533) diffraction peaks of Fe_3O_4 (JCPDS No. 19–0629), indicating the entire transformation to crystalline Fe_3O_4 at 550°C in Ar. The carbon content of Fe_3O_4-MC is 15%, but no typical peaks of crystal carbon were observed. This phenomenon may be ascribed to the extremely strong peaks of Fe_3O_4. For MC, the broad diffraction peaks at 22° and 43°Can be ascribed to MC (002) and (001) planes, respectively. The broad peaks also indicate MC are in the amorphous form.

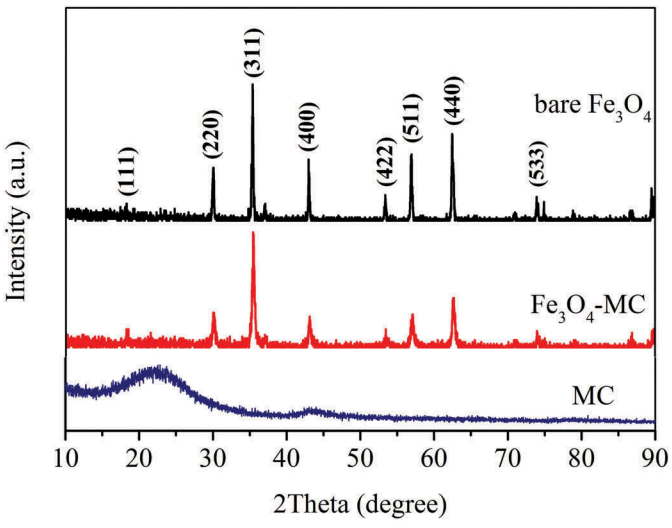

Figure 1. XRD patterns of bare Fe_3O_4, MAC and Fe_3O_4-MC composite.

Scanning electron microscopy (SEM) and energy-dispersive X-ray spectroscopy elemental (EDS) mapping was utilized to investigate the elemental distribution of Fe_3O_4-MC and MC. As shown in Figure 2(a), MC are composed of some larger particles and numerous small nanoparticles. Figure 2(b) indicates that the carbon elemental distribution is just like the particle shape in Figure 2(a). As shown in Figure 2(c), the particle morphology of Fe_3O_4-MC is very similar to that of MC (Figure 2(a)). While, the carbon elemental distribution is distinctly different from the particle shape in Figure 2(c). Fe and O element distribution (Figure 2(d,e)) is very similar and distributed through the whole view of the figure. These phenomena imply that MC are thoroughly covered by Fe_3O_4 nanoparticles. Even, some pore of MC may be filled by Fe_3O_4 nanoparticles.

Visual observation of morphology and structure was indicated by TEM (Figure 3). From the TEM image in Figure 3(a), the bare Fe_3O_4 particles are highly agglomerated, exhibiting irregular morphology and large size in the range of 100–900 nm, whereas Fe_3O_4-MC composite shows relatively homogenous morphology and small size in range of 20–100 nm (Figure 3(b)). These results indicate that Fe_3O_4 nanoparticles can be obtained by pyrolysis of ferric salt adsorbed MC. In addition, the MC could provide better electrical conductivity for the Fe_3O_4 nanoparticles.

The porosities of MC and Fe_3O_4-MC composite were estimated by N_2 adsorption-desorption experiments and the isotherms are showed in Figure 4(a). The Brunauer-Emmett-Teller (BET) surface area of Fe_3O_4-MC composite is calculated to be about 253.3 $m^2 \cdot g^{-1}$, which is higher than that of previously reported Fe_3O_4-based materials. Such a high special surface area for composite is conducive to increasing the contact area between active materials and electrolyte and providing more active paths for the rapid mass diffusion of electrolyte [31,32]. The pore volume of Fe_3O_4-MC composite drops to 0.32 $cm^3 \cdot g^{-1}$, compared with 1.12 $cm^3 \cdot g^{-1}$ of MC. It reveals that Fe_3O_4 is successfully inset into the pores of MC. The pore size distribution (Figure 4(b)) calculated using the Barret-Joyner-Halenda (BJH) method demonstrates that the main pore size of Fe_3O_4-MC composite and MC range from 2 to 12 nm mainly centered at 3 nm, indicating that pores of two samples are mainly mesopores. Notably, Fe_3O_4-MC composite also contains amounts of pores from 40 nm to 80 nm. The largest pore size of Fe_3O_4-MC composite is 121 nm, which is completely lower than that of MC (226 nm). Compared to MC, Fe_3O_4-MC composite has a narrow pore size distribution, which could be ascribed to some lager pores of MC filled by Fe_3O_4. The porous structure of Fe_3O_4-MC composite will be beneficial for retaining electrolyte and providing buffer lithium ions for rapid electrochemical reactions, resulting in relatively high capacity and good cycling performance.

To investigate the electrochemical behavior of the as-prepared bare Fe_3O_4 and Fe_3O_4-MC composite, coin cells

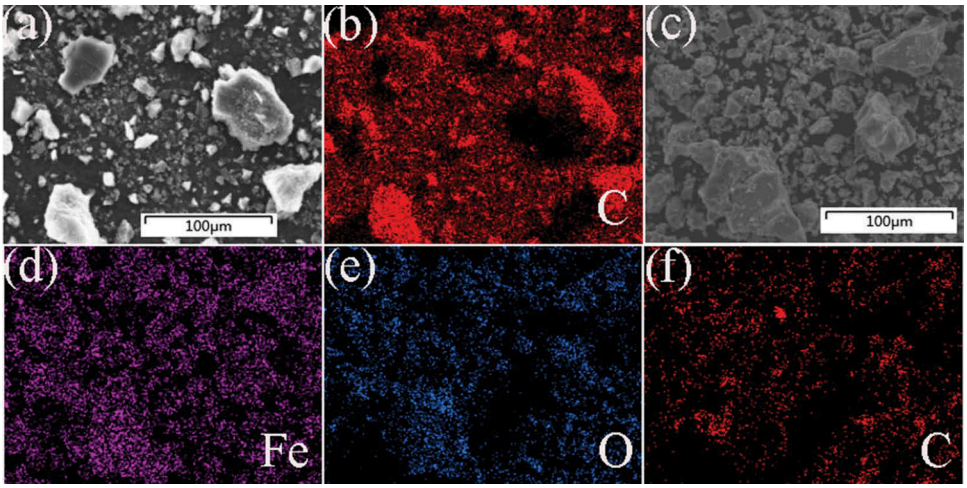

Figure 2. SEM images of (a) MC and (c) Fe_3O_4-MC composite. The distributions of C (b) at the whole MC. The distributions of Fe (d), O (e) and C (f) at the whole Fe_3O_4-MC composite.

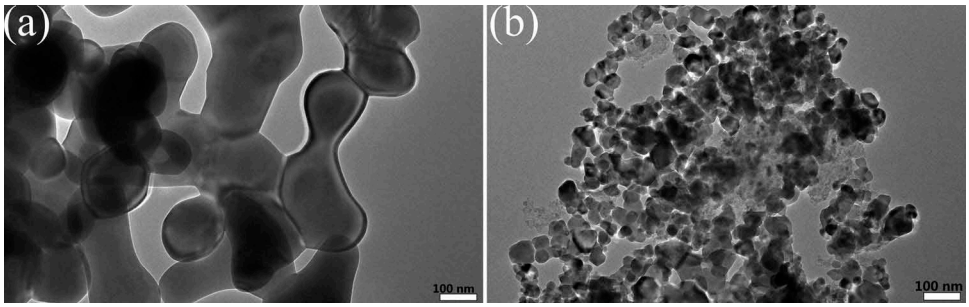

Figure 3. TEM images of (a) bare Fe_3O_4 and (b) Fe_3O_4-MC composite.

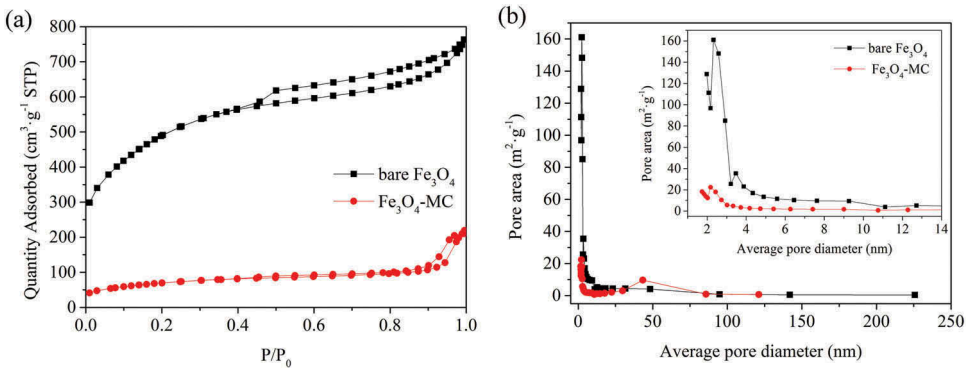

Figure 4. (a) N_2 adsorption-desorption isotherms of MC and Fe_3O_4-MC composite. (b) Pore size distribution of MC and Fe_3O_4-MC composite.

CR2032 are assembled with lithium foil as the counter electrode. Figure 5 shows the charge-discharge voltage profiles of bare Fe_3O_4 and Fe_3O_4-MC composite for the 1st (a) and 5th (b) cycles at the current density of 100 mA· g^{-1} between 0.0 and 3.0 V. As shown in Figure 5(a), the discharge and charge capacities of bare Fe_3O_4 are1038 and 716 mAh· g^{-1} for the first cycle, respectively, while Fe_3O_4-MC composite delivers higher discharge and charge capacities (1314 and 897 mAh· g^{-1}), resulting in the initial columbic efficiency of around 69.0% and 68.3%, respectively. The irreversible capacity loss may be due to the formation of SEI layer and other irreversible reactions. The slightly lower initial columbic efficiency of Fe_3O_4-MC composite is attributed to adverse effect from high specific surface area [33]. The fifth charge-discharge capacities of bare Fe_3O_4 are 610 and 638 mAh· g^{-1}, while those of Fe_3O_4-MC composite are 920 and 943 mAh· g^{-1}, respectively. Therefore, the fifth coulombic efficiency of bare Fe_3O_4 and Fe_3O_4-MC composite is 95.6% and 97.6%, respectively. The fifth coulombic efficiency of Fe_3O_4-MC composite is higher that of bare Fe_3O_4. During the first cycle, the obvious discharge voltage plateaus can be observed around 0.8V, which then migrates towards about 1.0V in the following cycles (see Figure 5(b)), indicative of the reduction of Fe_3O_4, i.e.

$Fe_3O_4+8e^-+8Li^+3Fe^0+4Li_2O$ [21].

The electrochemical performance of bare Fe_3O_4 and Fe_3O_4-MC composite electrode was evaluated using cyclic voltammograms (CVs) recorded for the first (Figure 6(a)) and third (Figure 6(b)) with a scan rate of 0.1 mV s^{-1}. As shown in Figure 6(a), two distinct reduction peaks of bare Fe_3O_4, located at 0.48 V and 0.27 V were observed, while two well-defined peaks of Fe_3O_4-MC composite around 0.78 V and 0.55 V were founded, corresponding to lithium insertion to form $Li_xFe_3O_4$ (Fe_3O_4 + xLi^+ + xe^- →

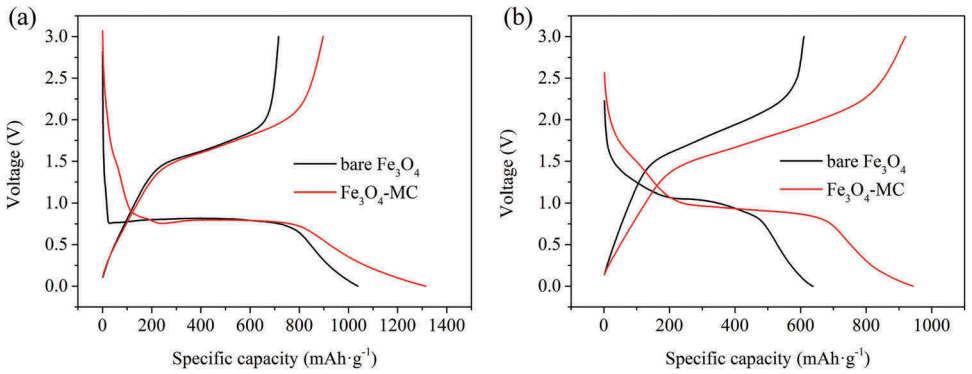

Figure 5. The charge-discharge voltage profiles of bare Fe_3O_4 and Fe_3O_4-MC composite at a current density of 100 mA· g^{-1} **a** initial, **b** fifth.

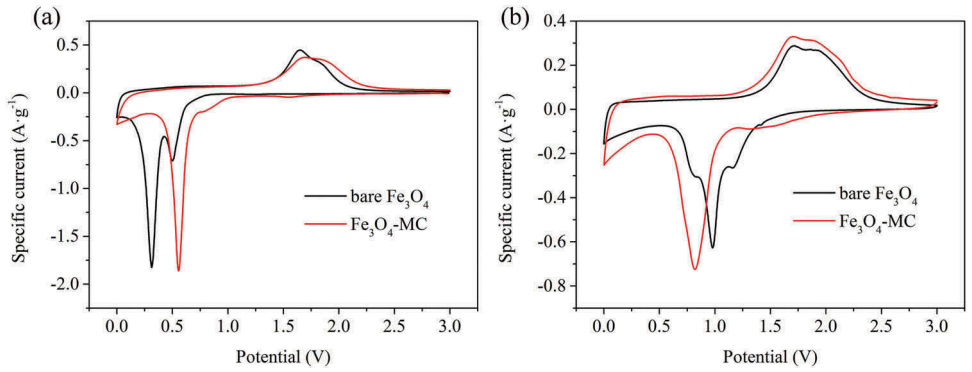

Figure 6. Cyclic voltammograms (CVs) of bare Fe_3O_4 and Fe_3O_4-MC composite at a scanning rate of 0.1 mV s^{-1} (a) first cycle and (b) third cycle.

$Li_xFe_3O_4$) and gradual reduction of Fe^{3+}/Fe^{2+} to Fe° and the formation of solid electrolyte interface (SEI) layer ($Li_xFe_3O_4$ + (8-x)Li^+ + (8-x)e^- → $4Li_2O$ + 3Fe) [31,32]. In the subsequent cycles (Figure 6(b)), these reduction peaks obviously shift to a higher potential of about 1.0 V, demonstrating the occurrence of structural changes in Fe_3O_4 nanoparticles after lithium intercalation in the first cycle [31]. For the oxidation peaks (Figure 6(a,b), the anodic peaks about 1.75 V for bare Fe_3O_4 and Fe_3O_4-MC composite are ascribed to the oxidation of Fe° to Fe^{2+}/Fe^{3+}. More important, CV curves of Fe_3O_4-MC composite own a much larger area than bare Fe_3O_4 in the third cycle, which implies a much higher capacity of Fe_3O_4-MC composite.

The rate performances of bare Fe_3O_4 and Fe_3O_4-MC composite evaluated and the result is exhibited in Figure 7. The reversible capacities of bare Fe_3O_4 and Fe_3O_4-MC composite are kept at 610 and 920 mAh· g^{-1} after the 5th cycle at 100 mA· g^{-1}, respectively. With the current density increasing, the specific capacities of the two samples drop gradually. At the current density of 1500 mA· g^{-1}, the charge capacities of bare Fe_3O_4 stabilizes at 196 mAh· g^{-1} while the Fe_3O_4-MC composite even stabilizes at 281 mAh· g^{-1}. Apparently, the charge capacity of Fe_3O_4-MC composite is completely superior to that of bare Fe_3O_4. From Figure 7, Fe_3O_4-MC composite exhibits better rate performance than bare Fe_3O_4, which is due to the existence of mesoporous activated carbon in Fe_3O_4-MC composite, allowing rapid transfer of lithium ions.

The cycling performance of bare Fe_3O_4 and Fe_3O_4-MC composite were also measured at 600 mA· g^{-1} and Figure 8 shows their comparison. The initial charge capacity of bare Fe_3O_4 and Fe_3O_4-MC composite are 646 mAh· g^{-1} and 796 mAh· g^{-1}, respectively. The introduction of mesoporous carbon reduces the size of Fe_3O_4 nanoparticles. SEM have

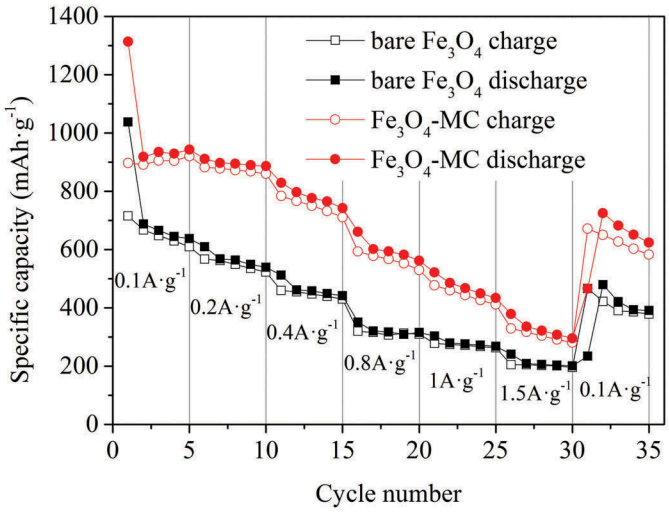

Figure 7. Rate capability of bare Fe_3O_4 and Fe_3O_4-MC composite at different current densities.

proved that the vast majority of Fe_3O_4 nanoparticles are attached on MC particles, which is different from the Fe_3O_4 nanoparticles covered by mesoporous carbon sphere [34]. The surrounding mesopores and carbon matrix buffer the volume expansion/contraction of Fe_3O_4 nanoparticles and thus Fe_3O_4 nanoparticles covered by mesoporous carbon sphere show good cycling performance. However, Fe_3O_4-MC composite are prepared by a simple one step and vast majority of Fe_3O_4 nanoparticles are attached on MC particles. Fe_3O_4 nanoparticles attached on MC particles still tend to pulverize due to the huge volume expansion/contraction during the charge-discharge cycling. Thus, the capacities of Fe_3O_4 and Fe_3O_4-MC composite decrease rapidly before 50

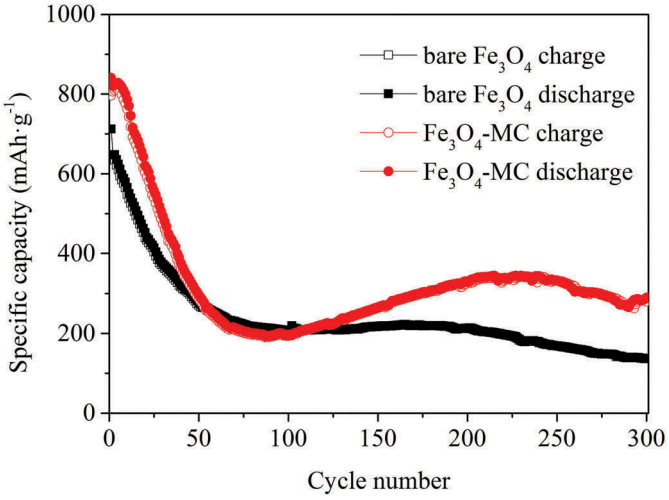

Figure 8. Cycling performance of bare Fe_3O_4 and Fe_3O_4-MC composite at 600 mA· g^{-1}.

cycles. After cycling 300 times, the charge capacity of bare Fe_3O_4 decreases to 136 mAh· g^{-1}. In contrast, Fe_3O_4-MC composite still remain the high charge capacity of 280 mAh· g^{-1} after 300 cycles. The capacity retention ratio of Fe_3O_4-MC composite is 35%, completely higher than that of bare Fe_3O_4, 21%. In comparison with the lowest charge capacity (190 mAh· g^{-1}) at the 87th cycle, the charge capacity of Fe_3O_4-MC composite at the 300th cycle increased 47%. The phenomena have been commonly found in some researches [31–34].

In order to further comprehend the electrochemical behaviors, EIS are performed on bare Fe_3O_4 and Fe_3O_4-MC composite electrodes, as shown in Figure 9. All Nyquist plots are alike in shape, which is composed of one semicircle in high frequency domain and a linear tail in the low frequency region. The semicircle in middle-high frequency domain is assigned to the charge-transfer resistance (R_{ct}), while the inclined line in low frequency represents the Warburg resistance (Z_w) of lithium ions diffusion in the active material. Obviously, the size of semicircle for Fe_3O_4-MC composite electrodes (~ 179 Ω) is much smaller than that of bare Fe_3O_4 electrodes (~ 227 Ω), indicating that Fe_3O_4-MC composite electrodes display lower charge-transfer resistance. The electrolyte resistances (R_e) of Fe_3O_4-MC composite and bare Fe_3O_4 are 5.5 and 12.0 Ω, respectively. The low R_e of Fe_3O_4-MC composite could be attributed to the porous structure and larger specific area. Additionally, the appreciably steep slope also explains the faster and easier Li^+ diffusion inside Fe_3O_4-MC composite electrodes.

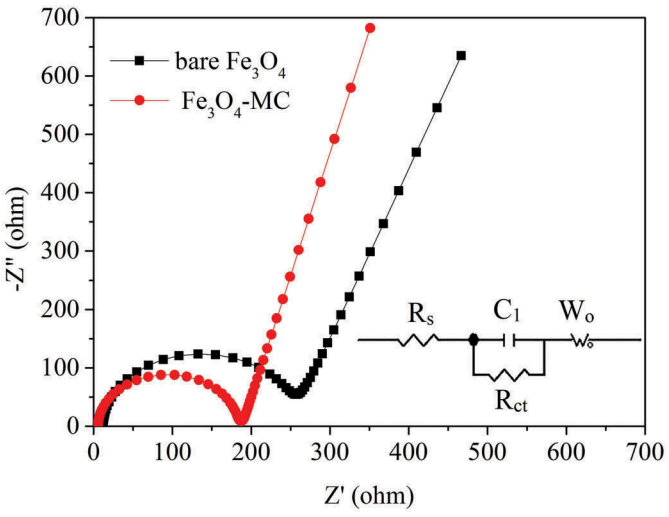

Figure. 9. Nyquist plots of bare Fe_3O_4 and Fe_3O_4-MC composite.

4. Conclusion

In summary, Fe_3O_4-MC composite was prepared by pyrolysis the $Fe(NO_3)_3 \cdot 9H_2O$ and $Fe(CH_3COO)_2 \cdot 4H_2O$ adsorbed MC. Fe_3O_4-MC composite shows higher reversible capacity of 920 mAh· g^{-1} and excellent rate performance (281 mAh· g^{-1} at 1500 mA· g^{-1}), compared to bare Fe_3O_4. XRD analysis proves that Fe_3O_4 crystals exist in the Fe_3O_4-MC composite. The SEM and EDS analysis indicate MC are covered by Fe_3O_4 nanoparticles. TEM illustrate that Fe_3O_4 nanoparticles can be obtained by using MC. BET analysis proves that the specific surface area of Fe_3O_4-MC composite is distinctly lower than that of MC, indicating some pores of MC are filled by Fe_3O_4 nanoparticles. In addition, Fe_3O_4-MC composite presents a high specific surface area (253.3 m^2· g^{-1}) and mainly mesoporous (pore size of 3 nm). The above unique structure is beneficial to improving the electrochemical performance of Fe_3O_4-MC composite.

Acknowledgments

This research was supported by the National Nature Science Foundation of China (No. 21466020).

Disclosure statement

No potential conflict of interest was reported by the authors.

Notes on contributors

Qingtang Zhang is working as an associate professor in the Department of Applied Chemistry, School of Petrochemical Engineering, Lanzhou University of Technology, Lanzhou, China. His research contribution is towards the area of eletrodes for lithium ion batteries. In his credit, he has published more than 20 international papers in the area of lithium ion batteries.Y. Meng is pursuing Mater research work in the Department of Applied Chemistry, School of Petrochemical Engineering, Lanzhou University of Technology, Lanzhou, China. Her research interest is in the field of Materials Science, especially for the anode materials of lithium ion Batteries.

Xiaomei Wang is working as a senior engineer in the State Key Laboratory of Advanced Processing and Recycling of Non-ferrous Metals, Lanzhou University of Technology, Lanzhou, China. Her research contribution is towards the area of eletrodes for lithium ion batteries.

References

[1] Tarascon J-M, Armand M. Nature. 2001;414:359–367.
[2] Armand M, Tarascon JM. Nature. 2008;451:652-657.
[3] Scrosati B, Garche J. J Power Sources. 2010;195:2419–2430.
[4] Wang Y, Liu B, Li Q, et al. J Power Sources. 2015;286:330–345.
[5] Deng D. Energy Sci Eng. 2015;3:385-418.
[6] Deng T, Zhou X. J Solid State Electrochem. 2016;20:2613–2618.
[7] Chen KF, Song SY, Liu F, et al. Chem Soc Rev. 2015;44:6230–6257.
[8] Poizot P, Laruelle S, Grugeon S, et al. Nature. 2001;32:496.
[9] Zhang L, Wu HB, Lou XW. Adv Energy Mater. 2014;4:1300958.
[10] Chen KF, Xue DF, Komarneni S. J Power Sources. 2015;275:136–143.

[11] Li KY, Chen H, Shua FF, et al. Electrochim Acta 2014. 136:10-18.
[12] Kang E, Jung YS, Cavanagh AS, et al. Adv Funct Mater. 2011;21:2430–2438.
[13] Abraham A, Housel LM, Lininger CN, et al. ACS Cent Sci. 2016;2:380–387.
[14] Jiang J, Li Y, Liu J, et al. Adv Mater. 2012;24:5166–5180.
[15] Liu G, Shao J, Gao Y, et al. J Solid State Electrochem. 2017;21:2593–2600.
[16] Xin Q, Gai L, Wang Y, et al. J Alloys Compd. 2017;691:592–599.
[17] Deng W, Ci S, Li H, et al. Chem Eng J. 2017;330:995–1001.
[18] He C, Wu S, Zhao N, et al. ACS Nano. 2013;7:4459-4469.
[19] Nguyen T-A, Kim IT, Lee S-W, et al. J Am Ceramic Soc. 2016;99:2720-2728.
[20] Hu A, Chen X, Tang Y, et al. Mater Lett. 2013;91:315–318.
[21] Li T, Bai X, Qi Y-X, et al. Electrochimica Acta. 2016;222:1562–1568.
[22] Yoon T, Chae C, Sun Y-K, et al. J Mater Chem. 2011;21:17325-17330.
[23] Jung B-Y, Lim H-S, Sun Y-K, et al. J Power Sources. 2013;244:177–182.
[24] Muraliganth T, Vadivel Murugan A, Manthiram A. Chem Communications. 2009;7360-7362.
[25] Xia H, Wan Y, Yuan G, et al. J Power Sources. 2013;241:486–493.
[26] Su DS, Schlogl R. ChemSusChem. 2010;3:136–168.
[27] Inagaki M, Konno H, Tanaike O. J Power Sources. 2010;195:7880–7903.
[28] Yang C, Lan JL, Liu W, et al. ACS Appl Mater Interfaces. 2017;9:18710–18719.
[29] Varma A, Mukasyan AS, Rogachev AS, et al. Am Chem Soc. 2016;116:14493-14586.
[30] Chen KF, Xue DF. Cryst Eng Comm. 2017;19:1230–1238.
[31] Ma C, Shi J, Zhao Y, et al. Chem Eng J. 2017;326:507–517.
[32] Wu Q, Zhao R, Liu W, et al. J Power Sources. 2017;344:74–84.
[33] Liu Y, Li P, Wang Y, et al. J Alloys Compd. 2017;695:2612-2618.
[34] Chen Y, Song B, Li M, et al. Adv Funct Mater. 2014;24:319–326.